ISSN:2790-1688 Volume-14-(2025)

The Effect of Geometries of Thin-Walled Parts on Residual Stresses and Deformations in SLM

Hongqiang Cai [a], Weishi Li [b]

School of Instrument Science and Opto-electronics Engineering, Hefei University of Technology, Hefei 230009, China.

[a] caihongqiang2022@163.com, [b] weishili@hfut.edu.cn

Abstract. Selective Laser Melting (SLM) technology demonstrates unique advantages in manufacturing complex thin-walled structures for aerospace and medical device applications, yet residual stresses during the forming process significantly compromise part accuracy and performance. This study systematically investigated the influence of geometric features on stress distribution and deformation mechanisms in thin-walled parts using 316L stainless steel powder through experiments. Three representative structures - polygonal tubes, elliptical tubes, and conical tubes - were analyzed, revealing that: polygonal tubes exhibit stress concentration at edges, which can be effectively mitigated by rounded transitions; elliptical tubes demonstrate a critical curvature effect where moderate curvature variations enhance precision; and conical tubes with inward-tilted structures significantly reduce deformation by altering heat accumulation effects. These findings provide important theoretical guidance for structural optimization of SLM-fabricated thin-walled components.

Keywords: Selective laser melting; Thin-walled parts; Residual stress; Deformation.

1. Introduction

With the rapid development of aerospace technology, the performance requirements for critical metal parts in modern aircraft have become increasingly stringent, with lightweight design, integrated structures, and multifunctional integration emerging as major trends [1,2]. However, traditional subtractive manufacturing processes face significant challenges in fabricating parts with complex geometries, e.g., thin-walled cavities, porous lattices. These methods not only suffer from inherent drawbacks such as low material utilization and time-consuming processing procedures, but also struggle to achieve high-precision, limiting the development and application of high-performance parts [3]. In contrast, additive manufacturing (AM) technology effectively overcomes the geometric constraints on the part of conventional manufacturing processes, providing an innovative solution for the fabrication of complex structural parts.

Among various AM techniques, selective laser melting (SLM) has become a key process for manufacturing precision metal parts in aerospace, biomedical, and other high-end fields [4,5]. However, the rapid melting and solidification during the forming process of SLM induce residual stresses, which often lead to part distortion or even cracking, significantly compromising geometric accuracy and mechanical properties [6-8]. Existing research showed that process parameters (e.g., laser power, scanning speed) [9,10], scanning strategies (e.g., island scanning, interlayer rotation) [11], and part geometry (e.g., wall thickness, curvature radius) [12-18] all influence the residual stress distribution and deformation behavior significantly.

In this paper, thin-walled specimens with representative geometries were designed and fabricated via SLM, followed by quantitative characterization of residual stresses and deformations using X-ray diffraction and three-dimensional scanning techniques to investigate the effect of geometries of thin-walled parts on residual stresses and deformations.

2. Materials and Methods

The experimental material was gas-atomized 316L stainless steel powder (average particle size 27.82 μm, sphericity >0.85), whose excellent corrosion resistance and oxidation resistance meet the application requirements in fields such as medical devices and marine engineering. Prior to fabrication, the powder was subjected to vacuum drying at 125°C for 2.5 hours to eliminate the influence of moisture on forming quality. The primary chemical composition is presented in Tab 1.

Tab 1. Chemical composition of 316L stainless steel powder

Chemical element	C	Si	Mn	Ni	Cr	Mo	S	P	Fe
Wt%	0.035	0.9	0.42	11.93	16.7	2.02	0.032	0.029	Bal.

The specimens were fabricated using a Renishaw AM250 metal 3D printer (build volume 250 × 250 × 300 mm, expandable to 360 mm). The machine is equipped with a 400W fiber laser (spot diameter 70–135 μm) and operates in an argon-protected environment, with a layer thickness of 20–50 μm and a forming accuracy of ± 0.1 mm.

A 67° interlayer rotation scanning strategy was adopted, with detailed process parameters listed in Tab 2.

Tab 2. Processing parameters used in SLM fabrication

Laser Power (w)	Layer Thickness (μm)	Scan Speed (mm/s)	Hatch Spacing (μm)	Laser BeamDiameter (μm)
200	30	1000	100	100

The experimental testing equipment is illustrated in Fig. 1. Geometric deformation were measured using a structured light scanning system (AICON StereoScan neo 3D), and the point cloud data were analyzed using Geomagic Qualify software (3D Systems, USA) to evaluate the deformation. Residual stress was characterized with a X-ray stress analyzer (Pulstec μ-X360s), employing the Debye ring method to evaluate surface stress. All measurements were performed after part removal from the build plate to ensure data reliability.

(a) StereoScan neo structured light scanner (b) μ-X360s portable X-ray residual stress analyzer

Fig. 1 Testing equipments

3. Results and Discussions

3.1 Thin-walled polygonal tubes

The first kinds of specimens investigated are tubes with regular polygonal cross-section. The height and wall thickness of specimens are 40 mm and 0.5 mm, respectively, with the number of edges of the polygon incrementally increased to approximate a circle with a diameter of 40 mm.

Tab 3 and Fig. 2 present the deformation contour maps and surface profile measurement results for different thin-walled polygonal tubes, respectively. The experimental results indicate that the

polygonal tubes generally exhibit an alternating convex/concave deformation pattern on adjacent surfaces, with maximum deformation concentrated in the central region of each face. As the number of the sides increases, deformation decreases significantly. The maximum deformation of the hexagonal and octagonal tubes decreased by 65% and 75%, respectively, compared to the quadrilateral tube. Note that the deformation of cylindrical tubes increased by 15% compared to the quadrilateral tube and this phenomenon need to be investigated furthermore.

Tab 3. Surface profile of SLM-fabricated thin-walled polygonal tubes

	Cross-section	Surface profile
Quadrilateral tube	Regular quadrilateral	1.0374 mm
Hexagonal tube	Regular hexagon	0.3655 mm
Octagonal tube	Regular octagon	0.2337 mm
Cylindrical tube	Circle	1.1273 mm

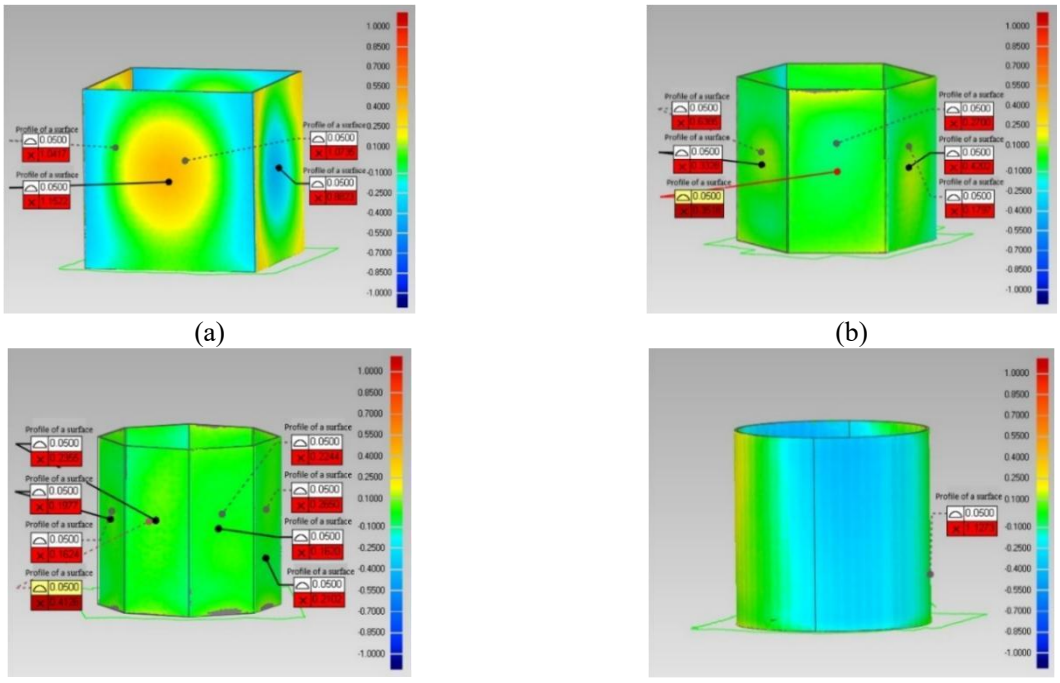

Fig. 2 Deformation distribution contour of SLM-fabricated thin-walled polygonal tubes

Based on the experimental characterization of deformation characteristics of the thin-walled polygonal tubes, this study selected thin-walled quadrilateral tubes as representative specimens for residual stress testing. As shown in Fig. 3, the measurement points were distributed in the central regions of both a convex surface (point1 to 5 in Fig. 3(a)) and a concave surface (point 11 to 15 in Fig. 3(b)), as well as the side regions of a convex surface (point 6 to 10 in Fig. 3(a)), where the building direction and the orthogonal direction on the surface are defined as 0° and 90° directions, respectively.

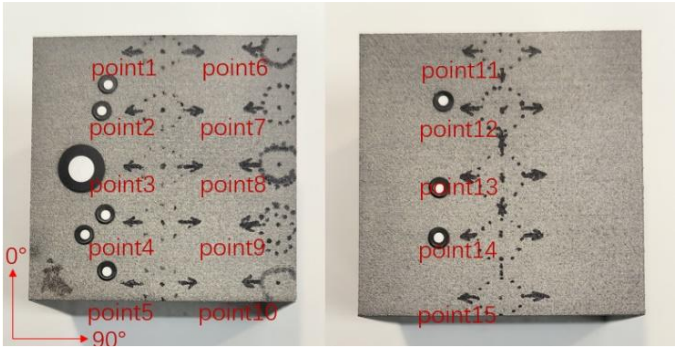

(a) (b)

Fig. 3 Residual stress measurement points on the thin-walled quadrilateral tube

The test results shown in Fig. 4 demonstrate that the central region of convex surfaces shown in Fig. 3(a) is under tensile stress, while the central region of concave surfaces is under compressive stress, with the maximum stress amplitudes all appearing in the most significantly deformed central areas. This stress distribution characteristic confirms the mechanism whereby tensile stress causes convex deformation and compressive stress induces concave deformation. Note that the maximum stress amplitudes in the side region are significantly higher than those in the central regions. Although direct measurement of edge stresses was not possible due to the limitation of the testing instrument, the high stress distribution in the side region verifies the existence of stress concentration at the edges.

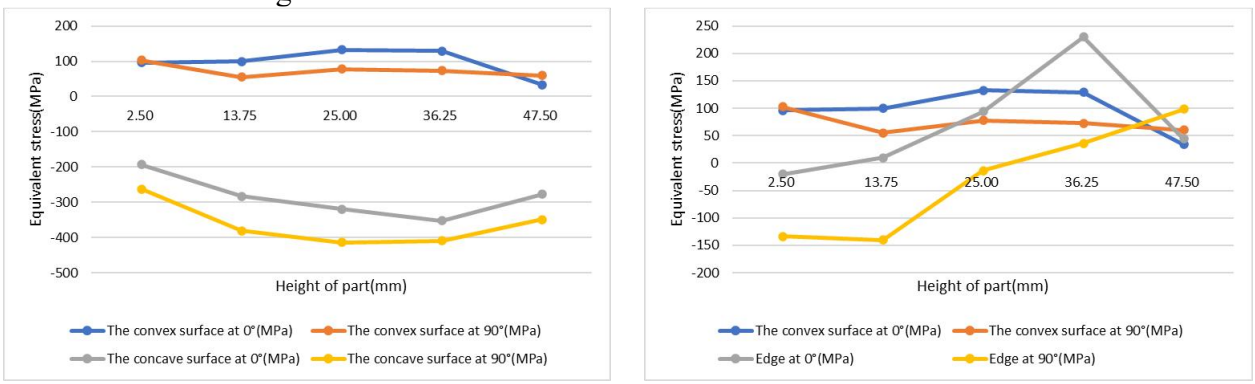

(a) (b)

Fig. 4 Stress components on the surface of the thin-walled quadrilateral tube

3.2 Thin-walled elliptical tubes

In metal additive manufacturing, a significant proportion of thin-walled components possess curved surface features. Elliptical tubes offer unique advantages as their curvature exhibits continuously varying characteristics, enabling the incorporation of multiple curvature states within a single component, making them particularly suitable for characterizing curvature's influence on the residual stress distribution and deformation characteristics. Therefore, the second kinds of specimens are thin-walled elliptical tubes. The height and wall thickness of all specimens are 40 mm and 0.5 mm, respectively, with a major axis of 60 mm. Continuous curvature variation was achieved by progressively reducing the minor axis from 60 mm to 10 mm.

Tab 4 and Fig. 5 present the deformation contour maps and surface profile measurement results for different thin-walled elliptical tubes. The experimental results demonstrate that while maintaining a constant major axis, when the minor axis dimension decreases from 60 mm to 40 mm, a convex deformation occurs at the bottom of the major axis side due to stress release, while the concave deformation on the minor axis side is alleviated with a 50% reduction in the maximum deformation. However, when the minor axis dimension is further reduced to 10 mm, a significant concave deformation zone appears in the middle-lower region of the minor axis side, accompanied with intensified convex deformation at the bottom of the major axis side, leading to a dramatic 296% increase in the maximum overall deformation. This phenomenon indicates that moderate curvature variations can improve the geometric accuracy of components, whereas excessive curvature changes will significantly exacerbate the deformation.

Tab 4. Surface profile of SLM-fabricated thin-walled elliptical tubes

	Minor axis	Surface profile
Elliptical tube a	60 mm	0.8240 mm
Elliptical tube b	50 mm	0.6815 mm
Elliptical tube c	40 mm	0.4111 mm

Elliptical tube d	30 mm	0.5478 mm
Elliptical tube e	20 mm	0.8169 mm
Elliptical tube f	10 mm	1.6267 mm

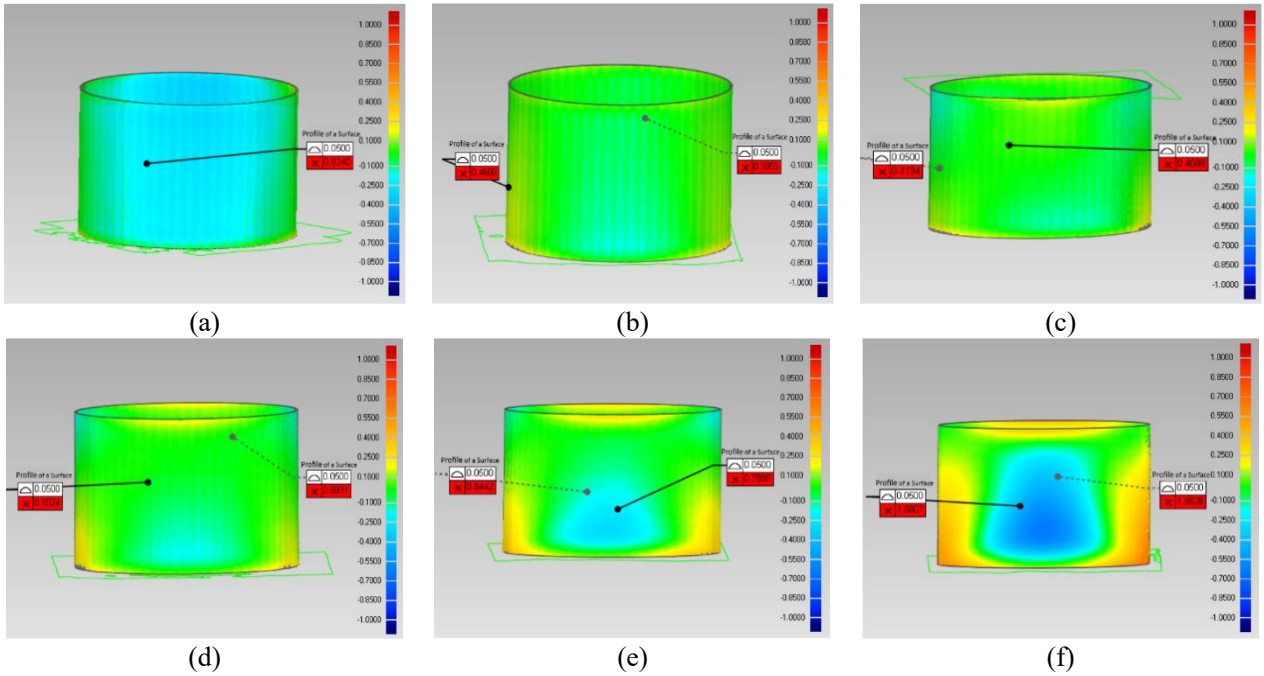

(a) (b) (c)

(d) (e) (f)

Fig. 5 Deformation distribution contour of SLM-fabricated thin-walled elliptical tubes

Based on the experimental characterization of deformation characteristics of thin-walled elliptical tubes, the thin-walled cylindrical tube and a thin-walled elliptical tube (major axis: 60 mm, minor axis: 10 mm) are selected as representative specimens for residual stress testing. As shown in Fig. 6(a), the measurement points for thin-walled cylindrical tubes were distributed in a concave deformation region (point 1 to 5) and an adjacent convex deformation region (point 6 to 10), while for the thin-walled elliptical tube, the measurement points are distributed on the major axis side (point 1 to 5) and minor axis side (point 6 to 10) as shown in Fig. 6(b).

The test result shown in Fig. 7(a) demonstrate that the convex deformation zone is primarily under tensile stress in the 0° direction, while the concave deformation zone is mainly under compressive stress in the 90° direction in thin-walled cylindrical tubes. For the thin-walled elliptical tube, the stress amplitude on the major axis side is significantly higher than that on the minor axis side as shown in Fig. 7(b). Specifically, the middle-lower region of the major axis side is mainly under tensile stress in the 0° direction, corresponding to convex deformation at the bottom, while the middle-upper region is mainly under compressive stress in the 90° direction, leading to concave deformation at the top. On the minor axis side, the tensile stress in the 0° direction shows a monotonically increasing trend with height, while the compressive stress in the 90° direction first increases and then decreases. These results not only verify the general principle that the stress in the 0° direction controls convex deformation while the stress in the 90° direction governs concave deformation, but also reveal that the stress distribution inhomogeneity caused by curvature differences is a critical factor affecting the deformation of thin-walled components fabricated by SLM.

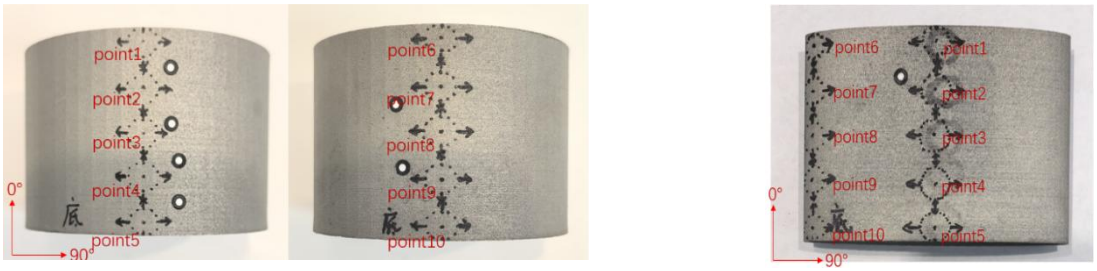

(a) Cylindrical tube (b) Elliptical tube

Fig. 6 Residual stress measurement points on thin-walled cylindrical and elliptical tubes

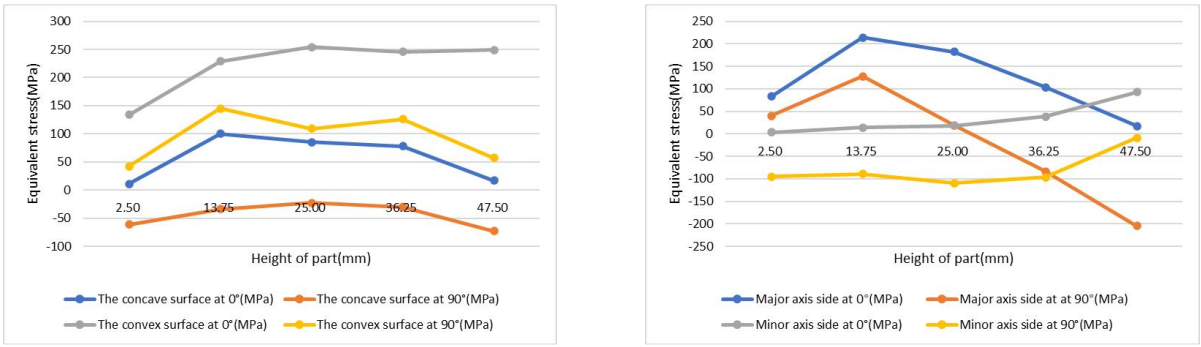

(a) Cylindrical tube (b) Elliptical tube

Fig. 7 Stress components in thin-walled cylindrical and elliptical tubes

3.3 Thin-walled conical tubes

The overhang feature inherent in thin-walled conical tubes is commonly observed in various complex components. Therefore, the third kinds of specimens considered in this paper are thin-walled conical tubes. The base diameter, height, and wall thickness of all specimens are 60 mm, 40 mm and 0.5 mm, respectively, while with variation of building directions and vertex angles (20° to 60°).

Tab 5 and Fig. 8 present the deformation contour maps and surface profile measurement result for different thin-walled conical tubes, respectively. The experimental results demonstrate that there are significant differences in deformation characteristics between the tubes fabricated with different building directions. As the vertex angle increases from 20° to 60°, the overall maximum deformation of thin-walled conical tubes fabricated from the big base to the small base decreases by 30.6% (from 0.9100 mm to 0.6318 mm), while that of the conical tubes turned up-side-down increases by 64.6% (from 1.4460 mm to 2.3800 mm). This remarkable difference originates from variations in heat accumulation effects caused by different building directions.

Tab 5. Surface profile of SLM-fabricated thin-walled conical tubes

	Cross-section	Surface profile
Conical tube a	10° inward inclination	0.8240 mm
Conical tube b	20° inward inclination	0.6815 mm
Conical tube c	30° inward inclination	0.4111 mm
Conical tube d	10° outward inclination	0.5478 mm
Conical tube e	20° outward inclination	0.8169 mm
Conical tube f	30° outward inclination	1.6267 mm

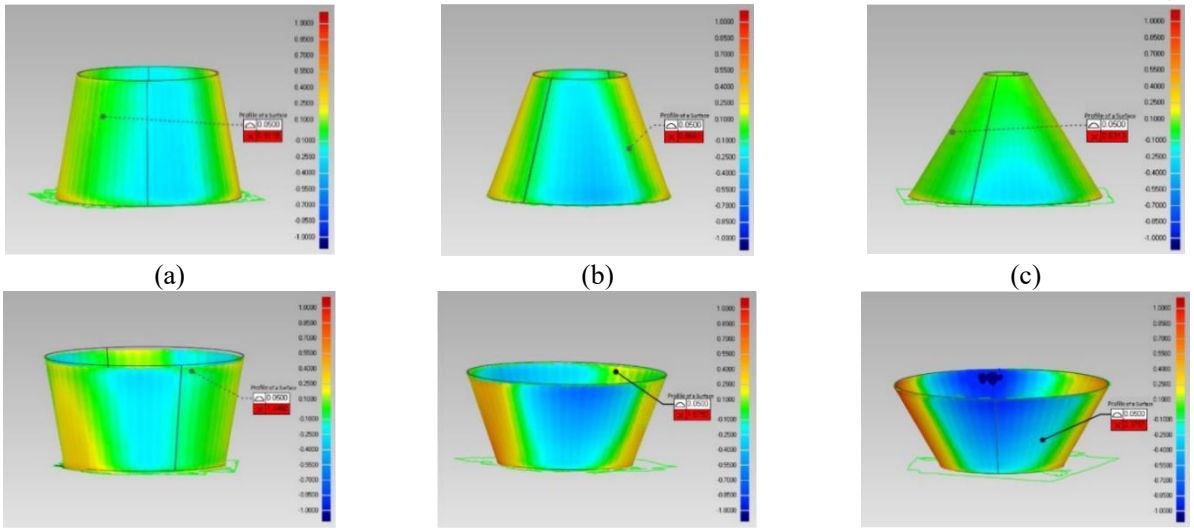

(a) (b) (c)

(d) (e) (f)

Fig. 8 Deformation distribution contour of SLM-fabricated thin-walled conical tubes

Based on experimental characterization of deformation characteristics in thin-walled conical tubes, the conical tubes shown in Fig. 8(c) and (f) are selected as representative specimens for residual stress testing. As illustrated in Fig. 9, measurement points were distributed across concave deformation zones and adjacent convex deformation regions of the thin-walled conical tubes.

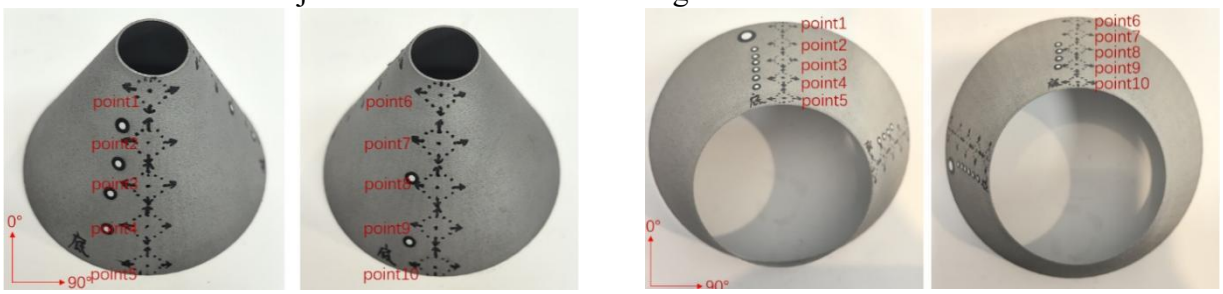

(a) Inwardly inclined conical tube (b) Outwardly inclined conical tube

Fig. 9 Residual stress measurement points on thin-walled conical tubes

The test results shown in Fig. 10 demonstrate that the inward-tilted conical tube is under compressive stress, with maximum stress amplitudes occurring in the central region. In contrast, the outward-tilted conical tube is mainly under tensile stress, with the maximum stress amplitude is about half of that observed in the inward-tilted one. This difference may be a result of the higher order deformation the outward-tilted one which means higher level of stress relief.

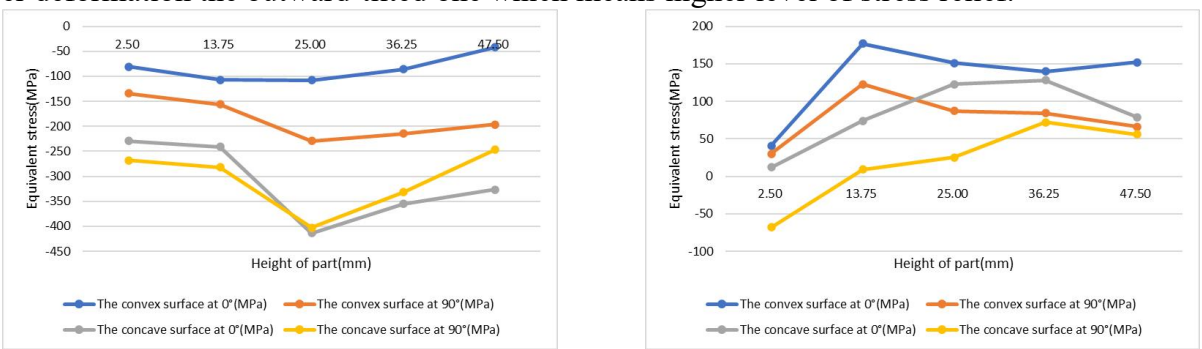

(a) Inwardly inclined conical tube (b) Outwardly inclined conical tube

Fig. 10 Stress components at 0° and 90° orientations in thin-walled conical tubes

4. Conclusions

In this paper, the residual stress distribution and deformation of three kinds of representative thin-walled structures have been quantitatively characterized with three-dimensional scanning and X-ray diffraction analysis and we found that:

(1) For polygonal tubular structures, adjacent surfaces exhibited distinct deformation patterns, i.e. one is convex and the adjacent one is concave. Tensile stress is dominated on the convex deformed surface, while compressive stress is dominated on the concave deformed surface. Furthermore, the deformation is reduced by 75% when the number of sides is increased from quadrilateral to octagonal, confirming the effectiveness of rounded transitions in suppressing deformation.

(2) For elliptical tubes, the deformation characteristics is curvature-dependent. The maximum deformation is decreased by 50% when the minor axis is reduce from 60mm to 40mm and the major axis is 60mm, however, when the minor axis is reduced to 10mm, the deformation is increased by 296% . Tensile stress is dominated along the building direction, and compressive stress is dominated along the orthogonal direction on the surface.

(3) The deformation characteristics of conical tubes is dependent on the building direction. When the conical tube is fabricated from the big base to the small base, the tube is under compressive stress, and tensile stress is dominated when the tube is turned up-side-down, resulting in increased deformation.

References

[1] Herzog D, Seyda V, Wycisk E, et al. Additive manufacturing of metals[J]. Acta Materialia, 2016, 117: 371-392.

[2] DebRoy T, Wei H L, Zuback J S, et al. Additive manufacturing of metallic components–process, structure and properties[J]. Progress in materials science, 2018, 92: 112-224.

[3] Rouf S, Malik A, Singh N, et al. Additive manufacturing technologies: Industrial and medical applications[J]. Sustainable Operations and Computers, 2022, 3: 258-274.

[4] Lu X, Zhao T, Ji X, et al. 3D printing well organized porous iron-nickel/polyaniline nanocages multiscale supercapacitor[J]. Journal of Alloys and Compounds, 2018, 760: 78-83.

[5] Zheng M, Wei L, Chen J, et al. A novel method for the molten pool and porosity formation modelling in selective laser melting[J]. International Journal of Heat and Mass Transfer, 2019, 140: 1091-1105.

[6] Jin W, Zhang C, Jin S, et al. Wire arc additive manufacturing of stainless steels: a review[J]. Applied sciences, 2020, 10(5): 1563.

[7] Kruth J P, Froyen L, Van Vaerenbergh J, et al. Selective laser melting of iron-based powder[J]. Journal of materials processing technology, 2004, 149(1-3): 616-622.

[8] Guoqing C, Binggang Z, Wei L, et al. Crack formation and control upon the electron beam welding of TiAl-based alloys[J]. Intermetallics, 2011, 19(12): 1857-1863.

[9] Thijs L, Verhaeghe F, Craeghs T, et al. A study of the microstructural evolution during selective laser melting of Ti–6Al–4V[J]. Acta materialia, 2010, 58(9): 3303-3312.

[10] Carter L N, Martin C, Withers P J, et al. The influence of the laser scan strategy on grain structure and cracking behaviour in SLM powder-bed fabricated nickel superalloy [J]. Journal of Alloys and Compounds, 2014, 615: 338-47.

[11] Venturi F, Taylor R. Additive manufacturing in the context of repeatability and reliability[J]. Journal of Materials Engineering and Performance, 2023, 32(15): 6589-6609.

[12] Qi H, Lee B, Gao Y, et al. Studies of thermal distortion and residual stresses of an Inconel 718 part fabricated by the laser powder deposition process[C]//ICALEO 2008: 27th International Congress on Laser Materials Processing, Laser Microprocessing and Nanomanufacturing. AIP Publishing, 2008.

[13] Gao S, Tan Z, Lan L, et al. Effects of geometrical size and structural feature on the shape-distortion behavior of hollow Ti-alloy blade fabricated by additive manufacturing process[J]. Journal of Laser Applications, 2020, 32(3).

[14] Jayanath S, Achuthan A. A computationally efficient hybrid model for simulating the additive manufacturing process of metals[J]. International Journal of Mechanical Sciences, 2019, 160: 255-269.

[15] Chen C, Zhu H, Xiao Z, et al. The residual stress distribution of Ti-6Al-4V thin wall in the selective laser melting[C]//IOP Conference Series: Materials Science and Engineering. IOP Publishing, 2019, 538(1): 012020.

[16] Lu X, Chiumenti M, Cervera M, et al. Warpage analysis and control of thin-walled structures manufactured by laser powder bed fusion[J]. Metals, 2021, 11(5): 686.

[17] Vastola G, Sin W J, Sun C N, et al. Design guidelines for suppressing distortion and buckling in metallic thin-wall structures built by powder-bed fusion additive manufacturing[J]. Materials & Design, 2022, 215: 110489.

[18] An K, Yuan L, Dial L, et al. Neutron residual stress measurement and numerical modeling in a curved thin-walled structure by laser powder bed fusion additive manufacturing[J]. Materials & design, 2017, 135: 122-132.